Thermoresponsive Iron Oxide Nanocubes for an Effective Clinical Translation of Magnetic Hyperthermia and Heat-Mediated Chemotherapy

Binh T. Mai,[†,‡,⊥] Preethi B. Balakrishnan,[†,‡,⊥] Markus J. Barthel,[†] Federica Piccardi,[†] Dina Niculaes,[†,‡] Federica Marinaro,[†,#] Soraia Fernandes,[†] Alberto Curcio,[†] Hamilton Kakwere,[†] Gwennhael Autret,[§] Roberto Cingolani,[†] Florence Gazeau,[‖] and Teresa Pellegrino*,[†]

[†]Istituto Italiano di Tecnologia, via Morego 30, 16163 Genoa, Italy
[‡]Dipartimento di Chimica e Chimica Industriale, Università di Genova, Via Dodecaneso, 31, 16146 Genova, Italy
[§]Centre de Recherche Cardiovasculaire de Paris 56, rue Leblanc, 75737 Paris Cedex 15, France
[‖]Laboratoire Matière et Systèmes Complexes, UMR 7057, CNRS and University Paris Diderot, 75205 Paris Cedex 13, France

Ⓢ *Supporting Information*
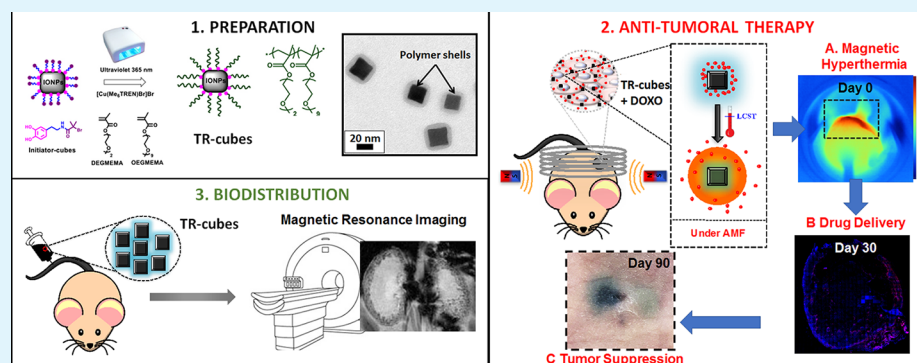
ABSTRACT: The use of magnetic nanoparticles in oncothermia has been investigated for decades, but an effective combination of magnetic nanoparticles and localized chemotherapy under clinical magnetic hyperthermia (MH) conditions calls for novel platforms. In this study, we have engineered magnetic thermoresponsive iron oxide nanocubes (TR-cubes) to merge MH treatment with heat-mediated drug delivery, having in mind the clinical translation of the nanoplatform. We have chosen iron oxide based nanoparticles with a cubic shape because of their outstanding heat performance under MH clinical conditions, which makes them benchmark agents for MH. Accomplishing a surface-initiated polymerization of strongly interactive nanoparticles such as our iron oxide nanocubes, however, remains the main challenge to overcome. Here, we demonstrate that it is possible to accelerate the growth of a polymer shell on each nanocube by simple irradiation of a copper-mediated polymerization with a ultraviolet light (UV) light, which both speeds up the polymerization and prevents nanocube aggregation. Moreover, we demonstrate herein that these TR-cubes can carry chemotherapeutic doxorubicin (DOXO-loaded-TR-cubes) without compromising their thermoresponsiveness both in vitro and in vivo. In vivo efficacy studies showed complete tumor suppression and the highest survival rate for animals that had been treated with DOXO-loaded-TR-cubes, only when they were exposed to MH. The biodistribution of intravenously injected TR-cubes showed signs of renal clearance within 1 week and complete clearance after 5 months. This biomedical platform works under clinical MH conditions and at a low iron dosage, which will enable the translation of dual MH/heat-mediated chemotherapy, thus overcoming the clinical limitation of MH: i.e., being able to monitor tumor progression post-MH-treatment by magnetic resonance imaging (MRI).

KEYWORDS: *magnetic hyperthermia, thermoresponsive polymer, drug delivery, cancer therapy, combined chemotherapy, doxorubicin*

INTRODUCTION

Oncothermia uses heat to shrink solid tumors, but the deposition of the localized heat remains the major challenge to overcome with regard to finding an effective treatment plan.[1−3] Doxorubicin (DOXO) is among the most widely used clinical chemotherapeutic agents to treat different tumors including breast, prostate, gastric, a wide variety of adenocarcinomas, etc.[4,5] DOXO suffers from nonspecific drug toxicity.[6] Free DOXO and DOXO as a liposomal nanoformulation (Doxil) have been FDA approved for cancer
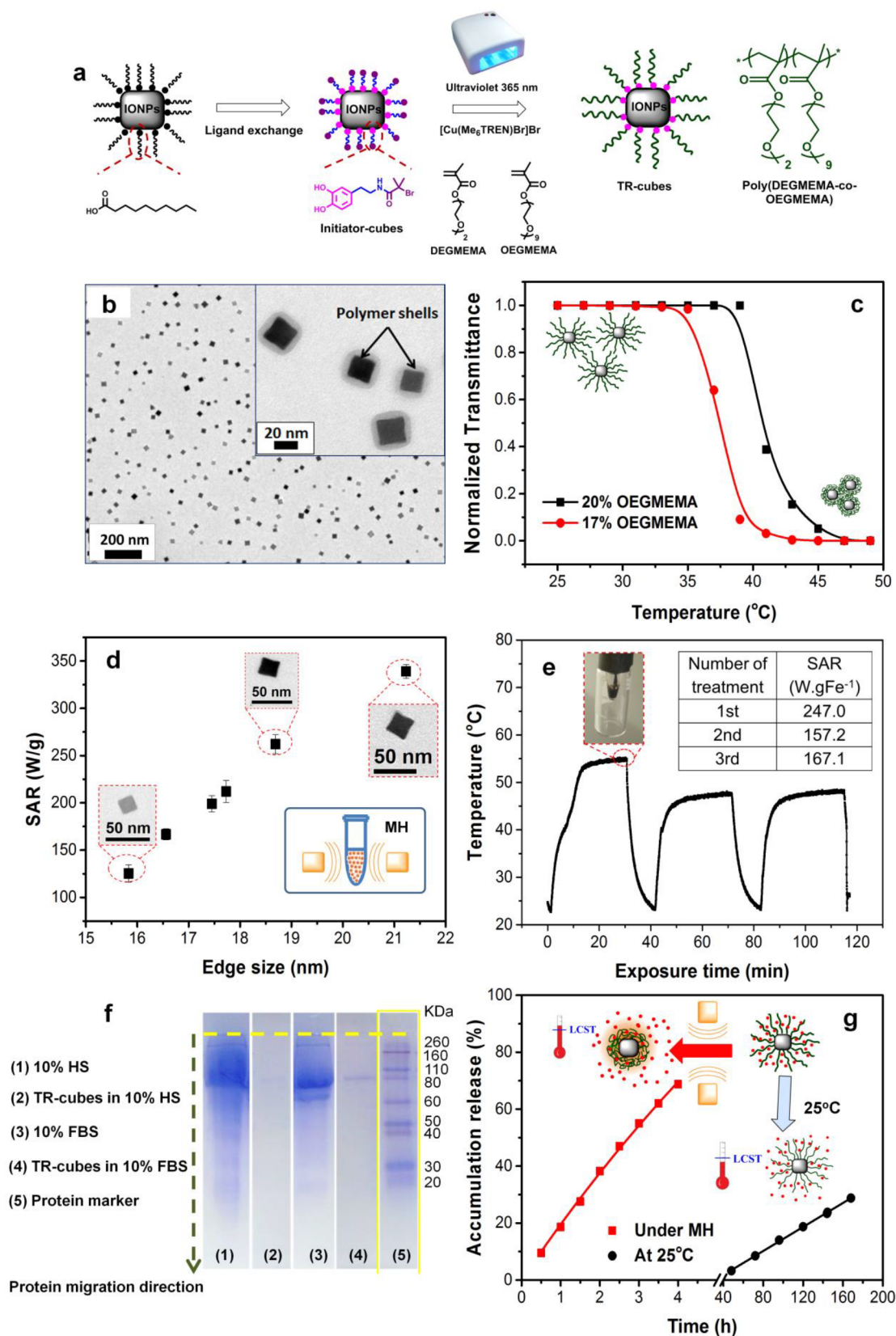
Figure 1. Synthesis and characterization of TR-cubes. (a) Illustration of the synthesis of TR-cubes by surface-initiated PI-CMRP. The polymerization, which is activated by a combination of UV light and a Cu(II) complex, enables a uniform and thick polymer shell to grow quickly on each nanocube. It also features oxygen tolerance and the need for a low amount of catalysts. (b) Representative TEM image of TR-cubes deposited from saline, showing the absence of aggregates. Inset: high-magnification image of TR-cubes with the clear presence of a polymer shell. (c) Transmittance vs temperature measurements of TR-cubes with 17% (red) and 20% (black) of OEGMEMA in the feeding molar ratio, resulting in two distinct lower critical solution temperatures (LCSTs) (37 and 42 °C, respectively). (d) SAR values as a function of TR-cubes at an increased

Figure 1. continued

cube edge size (black square) (11 kA m^{-1}, 105 kHz). (e) Heat profile of TR-cubes measured with an optical fiber (cube edge: 19.0 nm, 3.0 g of Fe L^{-1}, in saline) upon 3 cycles of 30 min treatment under MH. Inset: SAR values calculated for each of the three cycles of treatment. (f) Protein absorption assay using SDS-PAGE gel electrophoresis of TR-cubes in 10% fetal bovine serum (FBS) and 10% human serum (HS). (g) Profiles of cumulative DOXO release vs time at room temperature (black) and under MH (red). The accumulative releases reached 70% after 4 h under MH and 25% after 7 days at 25 °C.

treatment.[7] When chemotherapy is combined with hyperthermia, the dual treatment requires rigorous planning pertaining to the dosage, exposure time, and time interval between treatments in order to synergize actions while minimizing combined side effects, including drug resistance acquired by overdosed therapies.[8−12] Externally triggered nanomaterials may target heat more specifically and boost the drug release on demand.[13−16]

In magnetic hyperthermia (MH), magnetic nanoparticles (MNPs) can convert magnetic energy into heat under an alternating magnetic field (AMF).[2,12,17−19] Temperature-responsive coatings can undergo conformational changes and release previously entrapped drugs.[14,20−22] With regard to MNPs, the heat generated by the particles can activate the polymer shell (at the critical temperature) for an "on demand" drug delivery. For such a dual therapy that uses MNPs, temporal and spatial drug controls need to be achieved under clinically relevant MH conditions in order for it to progress to clinical translation.[15,23−26] Although it is extremely challenging to accomplish this, such nanoplatforms will help to reduce side effects.[27] In addition, given the high dose of materials used in clinics for MH and the non-degradability of current magnetic particles, which are made on purpose to enable multiple treatment cycles, magnetic resonance imaging (MRI) is not an appropriate imaging technique for following the progression of a tumor after MH treatment.[12,28] By combining the synergetic effect of MH and chemotherapy, our first aim is to reduce the dose of magnetic NPs. Furthermore, using a thermoresponsive polymeric coating that can slowly detach from the nanocube surface will facilitate the clearance of the nanocubes, thus enabling the use of MRI for monitoring the tumor progression.

In this work, we have chosen to use cubic-shaped nanoparticles that had been previously developed by some of us rather than standard spherical iron oxide nanoparticles because they are, to date, the most outstanding iron oxide based nanoparticles for use in magnetic hyperthermia.[28−30] Indeed, iron oxide nanocubes with cube edges of 17−21 nm possess specific absorption rate (SAR) values, the direct measure of their heating efficiency under AMF, that are among the highest values for iron oxide nanoparticles under clinical MH conditions.[28,29]

For the clinical translation of magnetic thermoresponsive iron oxide nanocubes (TR-cubes), the main challenge to overcome is maintaining both their thermoresponsiveness (in order to load and release the chemotherapeutic drug) and their high MH heat efficacy under in vivo conditions. This requires using single nanocubes, as the aggregation of the TR-cubes would hinder their heat performance.[21] At the transition between superparamagnetic and ferromagnetic regime, the heating capability of such IONCs depends on Brownian and Neil relaxation. Aggregation will impair the Brownian motion of single cubes and thus quench their heating capability.[31,32]

Within the 17−21 nm size range, which is optimal for heat dissipation, nanocubes exhibit magnetic interparticle interactions, rendering them difficult to modify. In a previous work,

we used reversible addition−fragmentation chain transfer polymerization (RAFT) to functionalize the cube surfaces with thermoresponsive poly(ethylene glycol methyl ether acrylate-*co*-N-isopropylacrylamide).[21] These nanomaterials featured a suitable transition temperature and capability to load and release DOXO, upon exposure to a clinically relevant AMF in a test tube. However, the formation of small aggregates/clusters of nanocubes during the polymerization resulted in a complete quenching of their heat performance when they were injected intratumorally in vivo into a murine model (data not shown). In a surface-initiated RAFT polymerization, the conventional initiator first decomposes in solution, and then the radicals undergo the chain transfer process on immobilized RAFTs at the nanocube to start a propagating chain polymerization. This delays the growth of the polymer on the surface, and the cubes could possibly interact to form small clusters. To improve the outcome of the functionalization, atom transfer radical polymerization (ATRP) was later used, since the initial step occurs directly at the nanocube surface.[33] However, the cubes underwent sedimentation soon after the injection of a high amount of a copper catalyst; thus, the stability of the TR-cubes upon the functionalization was found to be very low (see Figure S1 in the Supporting Information). Therefore, it is mandatory to keep nanocubes individually coated in order to maintain their high SAR values and preserve their optimal functional stimuli responsiveness. To fulfill these requirements, and to grow a thermoresponsive polymer shell on each individual cube, we developed a surface-initiated photoinduced copper-mediated radical polymerization (PI-CMRP) technique, which we used directly on the nanocubes.[34−36] In comparison to other radical polymerization techniques, PI-CMRP has three versatile features: it has an extremely fast polymerization rate, it possesses oxygen tolerance, and it uses a very low amount of catalyst.[36−38] These features simplify the polymerization process and enable a fast polymerization rate, making the protocol highly suitable for processing strongly interactive nanoparticles such as 17−21 nm nanocubes.

Finally, using the aforementioned PI-CMRP to obtain the TR-cubes (LCST ≈ 40 °C), we studied the efficacy of these heat hubs as mediators for magnetic hyperthermia therapy, alone and in combination with DOXO, which was loaded in the thermoresponsive shell. We did this on an in vivo xenograft tumor model using A431 epidermoid carcinoma cells, a tumor cell line that is sensitive to DOXO. We have further studied the in vivo biodistribution of the pristine TR-cubes at the dose needed for MH. With this study it is worth highlighting that, differently from many other studies done at MRI doses of iron oxide nanoparticles (50−100 μg$_{Fe}$/mouse), we have evaluated here the body tolerance and the clearance of these novel nanoplatforms at a dose needed for MH (0.5 or 1 mg$_{Fe}$/mouse) which is much higher than that needed for MRI.

■ RESULTS AND DISCUSSION

Polymer Growth. The synthetic approach is illustrated in Figure 1a. In a two-step approach, the hydrophobic ligands on the cubes were first replaced with catechol-based initiators, which subsequently initiated the polymerization from the cube surface. An ^{1}H NMR characterization of the initiator showed a product with a purity higher than 95% (see Figure S2). After ligand exchange, the nanocubes were found to be well dispersed in THF, while they were completely insoluble in CHCl$_3$; the latter is the best solvent for the pristine cubes, thus indicating a change in the chemistry at the nanocube surface. Next, upon the addition of monomers (diethylene glycol methyl ether methacrylate, DEGMEMA, and oligoethylene glycol methyl ether methacrylate, OEGMEMA), free initiators, and a copper catalyst to the initiator-modified nanocubes, exposure to UV light under nitrogen in a DMSO/THF solvent system (10% THF) resulted in polymer chain growth P(DEGMEMA-*co*-OEGMEMA)) on the nanocube surface (see Figure 1b and Figure S3 for polymer characterization). The [monomer]:[free initiator]:[CuBr$_2$]:[Me$_6$TREN]:[Fe] ratio used in this study was 10000:8.9:1:2:120. The free initiator molecules are needed to ensure that each nanocube has a large number of radicals. In addition, the exchanging halide atom between the immobilized and free initiators ensures that there is a low concentration of the initiating radicals that surround the surface.[33,39] This strengthens the controlled growth of the propagating chain via the suppression of radical coupling at the surface or interparticles.[33,39] The fast polymerization rate of PI-CMRP enabled the formation of a thick and uniform polymer shell on each nanocube, with an edge size of 19 nm or more, within only 2.5 h. For the characterization of the polymer we have used size exclusion chromatography (SEC) for molar mass determination and NMR for structural information (Figure S3). The unbounded polymer that was collected from the supernatant had a molar mass of 45000 g mol^{-1} and a narrow dispersity of 1.40, indicating that the polymer on the nanocube surface also grew in a controlled manner (Figure S3b). Furthermore, we observed that a longer polymerization time, up to 5 h, led to an increase in the molar mass to 250000 g mol^{-1}, while the dispersity of the chains increased to 1.84 (Figure S3). In addition, the ^{1}H NMR spectrum of the unbounded polymers confirmed a molecular structure consisting of polymethacrylic backbones with PEG pendants (Figure S3). The NMR signals from 4.20 to 3.20 ppm were assigned to the magnetic resonance of the proton in ethylene glycol based side chains (−O−CH$_2$−CH$_2$−O−, −O−CH$_3$). The signals from 1.05 to 0.60 ppm are assigned to the methylene protons (−CH$_2$−) in the polymer backbones, while the signals from 2.30 to 1.30 ppm are assigned to the methyl protons (−CH$_3$) in the polymer backbones. Please note that it is not possible to characterize the TR-cubes directly by NMR due to the presence of magnetic nanoparticles. Surprisingly, the colloidal stability and heat performance do not depend on the molar masses of the polymer chains (data are not shown here). Indeed, when we compared the SAR of the TR-cubes with that of the same nanocubes coated with molecules that had a nonthermoresponsive PEG shell, with a much lower molecular mass, we found that the heat performances of these differently coated nanocubes is very similar (Figure S4). This suggests that, if a polymer is able to provide the right colloidal stability and stabilize the nanocubes as individual entities, no matter

what its composition is, the heat performances will be maintained (Figure 1d and Figure S4).

To ensure in vivo kidney excretion, the cubes that had been functionalized with polymers with a molar mass of 45000 g mol^{-1} were selected. As expected, the uniformity and thickness of the polymer coating reduced the nanocube tendency to interact and aggregate (see the TEM of the well-dispersed TR-nanocubes, Figure 1b, and of the starting nanocubes, Figure S3). Furthermore, the dynamic light scattering (DLS) size of short ligand coated TR-cubes (i.e. the decanoic acid capped cubes in CHCl$_3$ and the initiator cubes in THF) showed that the hydrodynamic peaks are centered at 295 nm, and a major size reduction occurred for TR-cubes in a saline buffer (68 nm weighted by number, see the blue curve in Figure S5; the size weighted by intensity and volume can also be found in Figure S6). Furthermore, the polydispersive index of the TR-cubes measured in saline was as low as 0.16, which is in agreement with the value that was obtained for pristine IONCs measured in CHCl$_3$. Fourier transform infrared spectroscopy also demonstrated that the characteristic peaks are assignable to the newly introduced moieties when the surface composition is changed during each reaction step (Figure S5c). In detail, the characteristic absorption bands of the alkyl stretching (−C−H) at 2852−2952 cm^{-1} and carbonyl stretching (>C=O) at 1711 cm^{-1} were clearly visible for the initial cubic-IONPs coated with decanoic acid (black curve). Upon the ligand exchange, the alkyl stretching of the C−H group was significantly reduced. At the same time, the amide stretching (−NH) at 3398 cm^{-1} and the appearance of a peak at 1657 cm^{-1}, the latter attributed to the amide carbonyl stretching (−N−C=O) of the dopamine-bearing initiator group, indicated that most of the initial decanoic acid on the particle surface was replaced with an initiator (Figure S5c, blue curve). After the polymer growth step, the FT-IR spectrum of the TR-cubes showed characteristic groups of the polymer backbone. There were two strong peaks at 1716 and 1051 cm^{-1}, and these are ascribable to the ester carbonyl (−O−C=O) and ether (−C−O−C), indicating the growth of polymers at the nanocube surface (Figure S5c, red curve).

For the evaluation of the LCST, turbidimetric measurement is the standard characterization technique. This technique relies on changes in the transmittance (T) due to changes in the solubility of thermoresponsive polymers upon temperature variation. By recording of the transmittance of the TR-cube aqueous solution as a function of the temperature, the LCST of these nanohybrids can be determined by considering the inflection of the T vs temperature curve (Figure 1c). With the aim of achieving a phase transition temperature (LCST) above 37 °C, we first fixed the monomer composition at 17% OEGMEMA and 83% DEGMEMA,[40] which resulted in an LCST of 37 °C. The hydrophilic OEGMEMA monomer had to be increased to 20% to raise the LCST to 41 °C (Figure 1c). The absence of any aggregations after the nanocubes had been coated with the TR-shell was indirectly confirmed by the high SAR values that were recorded under clinical MH conditions (11 kAm^{-1}, 105 kHz).[41] The TR-cubes prepared here have a higher SAR value under clinical MH conditions in comparison to other systems reported so far in the literature.[42,43] The procedure was also applied to various cubes with sizes ranging from 15.8 to 21.2 nm, and the SAR values for different sized TR-cubes followed the same trend (Figure 1d) as that expected for the same cubes coated in a nonresponsive shell.[44,45] Moreover, 19 nm TR-cubes that had been exposed
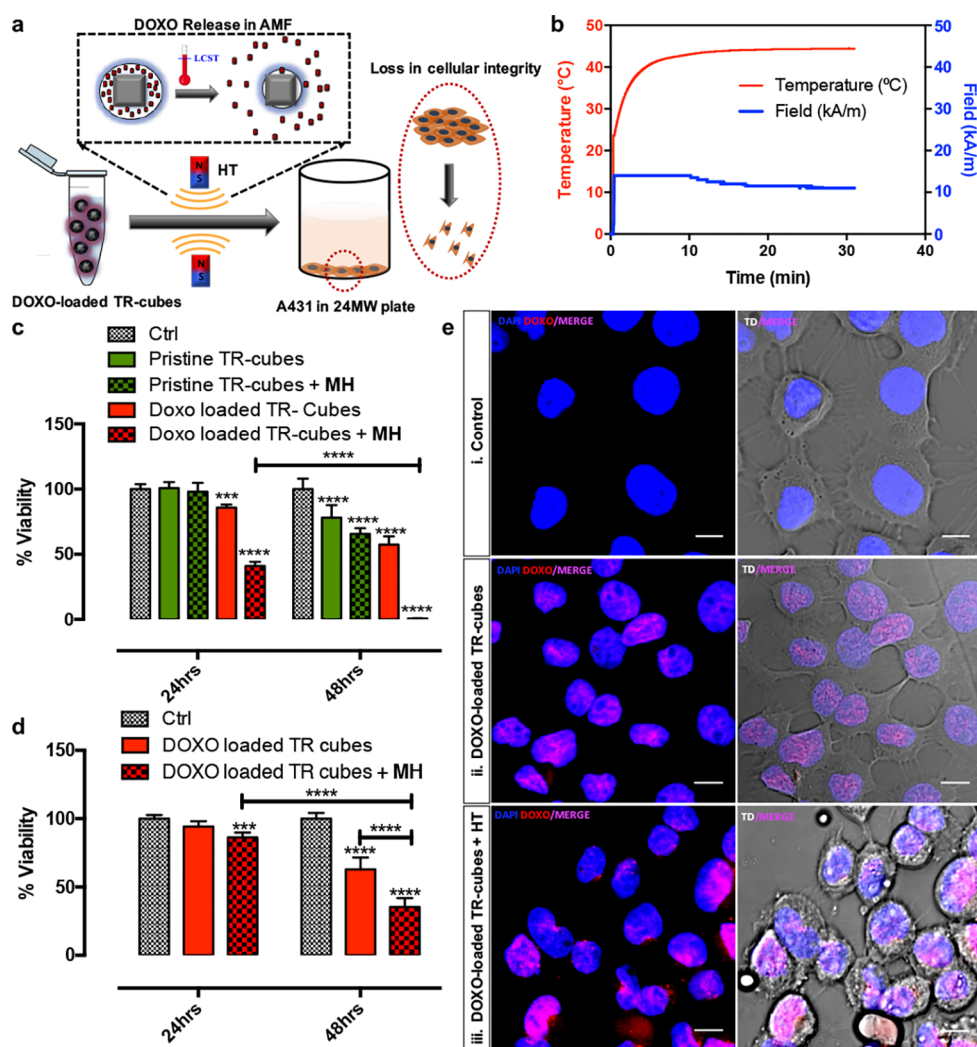
Figure 2. In vitro assessment of DOXO release and action for DOXO-loaded-TR-cubes. (a) Illustration of in vitro experiment conducted on A431 cells. (b) Temperature profile graph showing the rise in temperature up to 42 °C for DOXO-loaded-TR-cubes after 30 min under MH (11 kAm^{-1} and 110 kHz). (c, d) PrestoBlue toxicity results demonstrating a significant difference in the mean % toxicity of Ctrl untreated cells, cells treated with pristine TR-cubes, DOXO-loaded-TR-cubes, pre-MH treated pristine TR cubes, and pre-MH treated DOXO-loaded-TR-cubes after 24 and 48 h of incubation for 2.5 g/L Fe (c) and 1.5 g/L Fe (d) of nanocubes. $n = 3$, the error bar represents the standard deviation, and *** $p = 0.0001-0.001$ and **** $p < 0.0001$. (e) Confocal microscopic images taken after 4 h of incubation for control untreated A431 cells (i), cells treated with DOXO-loaded-TR-cubes (ii), and cells incubated with DOXO-loaded-TR-cubes pre-exposed to MH (iii), the last of which shows clear signs of cell stress and an improved DOXO uptake (intense violet signal). All of the left-hand panels display the DOXO channel in red and the channel for Hoechst 33342 stained nuclei in blue. The right-hand panels merge the left-hand panels with images that were obtained in transmission. All scale bars represent 50 μm.

to multiple MH cycles (three cycles) maintained a heat profile that was only a few degrees lower than that which was recorded after the first MH cycle (Figure 1e). The decrease in maximum temperature reached at the second and third MT cycles with respect to the first MH cycle may be due to the partial lack of polymer elasticity on the nanocube and to the formation of some small clusters once the TR-cubes are exposed to temperatures higher than the LCST (Figure 1e). The polymer shrinking may induce a partial nanocube aggregation, but this effect is only slight due to the temperature increase that is reached during the first, second, and third MH treatmenta in vivo.

Moreover, the antifouling feature of the OEG segments in the TR-cubes avoids protein opsonization, as was confirmed by an SDS-PAGE gel electrophoresis analysis of TR-cubes that had been exposed to a human serum (HS) or in the presence of fetal bovine serum (FBS) (Figure 1f and Materials and Methods for a detailed description).[46] This feature is required when nanoparticles are to be injected intravenously in order to prevent any obstruction or clogging of the blood vessels during circulation and to enable a long circulation time.

In Vitro Drug Loading and Release in a Test Tube. The chemotherapeutic agent, DOXO, was loaded onto the TR-cubes (DOXO-loaded-TR-cubes) by a nonspecific interaction just by mixing the TR-cubes with free DOXO in saline solution. After magnetic recovery, the DOXO loading capacity was estimated by a DMSO release experiment, and a ratio of 47 mg of DOXO for each 1 g of Fe of nanocubes has been measured (Figure S7 for the loading scheme, TEM, DLS, and heat profile). The DOXO loading did not affect the nanocube stability and the heat performance of the DOXO-loaded-TR-cubes. For the release profile, in a test tube, DOXO-loaded-
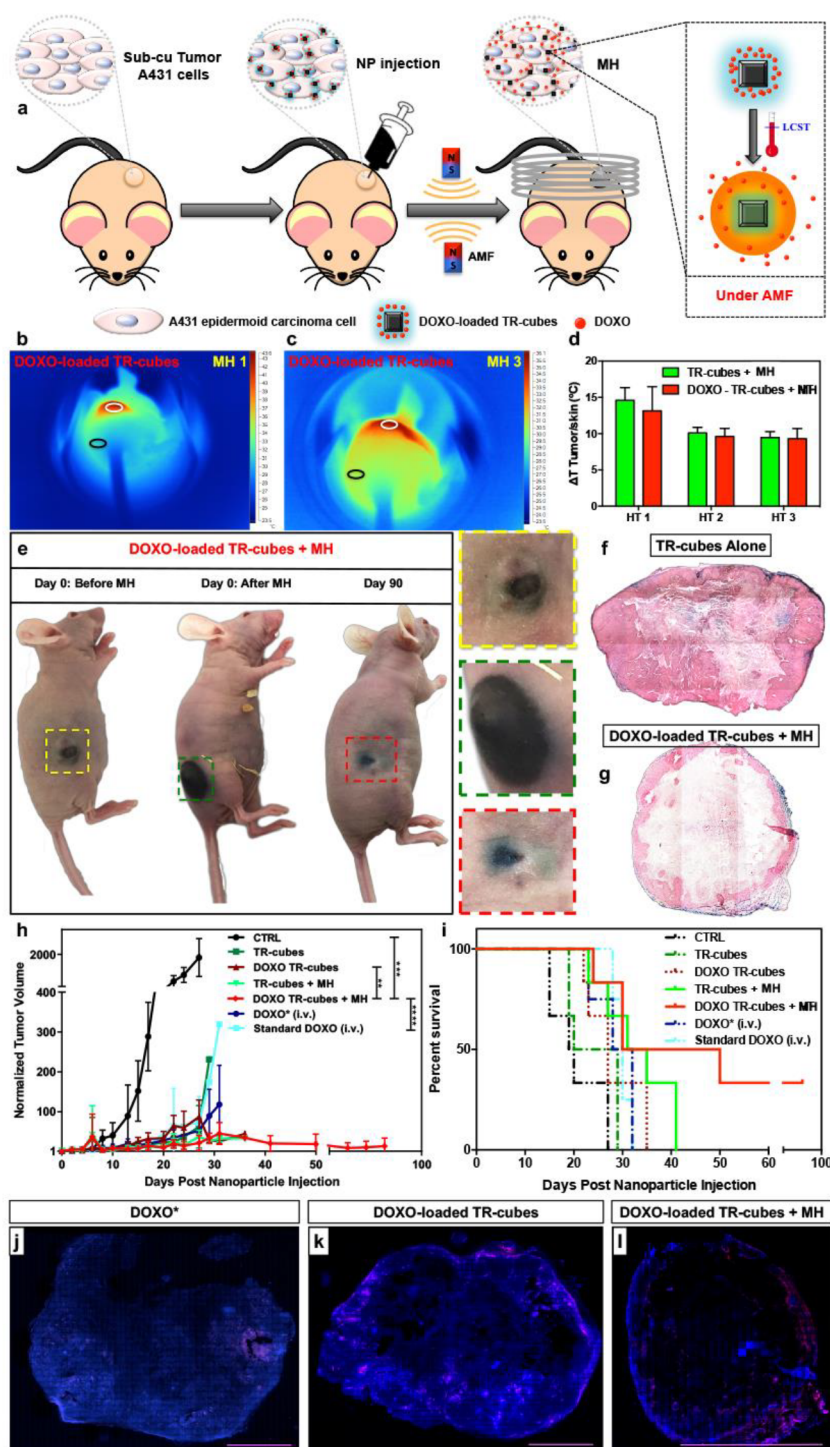
Figure 3. TR-cubes as an effective in vivo heat mediator and controlled drug delivery system. (a) Scheme of the in vivo efficacy study. (b, c) Infrared images showing the heating of DOXO-loaded-TR-cubes at day 1 (b, MH1) and day 3 (c, MH3). (d) Plot of the temperature difference (ΔT) between T_{Tumor} (white circle) and T_{Skin} (black circle), showing a 15 °C rise after MH1 and 10 °C after MH2 and MH3. (e) Photos of the animal after TR-cube injection (left animal), after the first MH cycles (middle), and at 90 days (right animal). Mice treated with DOXO-loaded-TR-cubes + MH showed complete tumor suppression by day 90 post-treatment (color coded inserts show enlarged images of the tumor). The photos of the three mice do not correspond to the same animal. (f, g) Histological sections of tumor treated with TR-cubes alone (f, intact stroma) or DOXO-loaded-TR-cubes + MH (g, thin stroma) stained with Prussian Blue for iron and Fast Red dye for collagen. (h, i) Tumor growth curve and Kaplan−Meier survival plot showing the difference in tumor suppression and improved survival between the DOXO-loaded-TR-cubes + MH and the other groups studied. The DOXO-loaded-TR-cubes + MH group in the tumor growth curve showed significant improvement in tumor suppression in comparison to the control group (with $p = 0.0002$ (***)), the standard DOXO group ($p < 0.0001$ (****)), and the DOXO-TR-cube group ($p = 0.0035$ (**)). (j−l) Confocal images of the whole tumor slice, which was sacrificed 30 days post treatment, showing the presence of viable cancer cells (DAPI blue staining) and DOXO (red signal, shown in pink due to the merge with DAPI) for DOXO* (j), DOXO-loaded TR-cubes (k), and DOXO-loaded TR-cubes + MH (l). The scale bar represents 0.5 cm.

TR-cubes were exposed to MH for 4 h and UV–vis absorption measurements were carried out on the supernatant after magnetic separation of the nanaocubes. The release profile of DOXO was boosted 3-fold in comparison to that which occurred at 25 °C: i.e., at room temperature (no MH, Figure 1g). After 4 h under MH, 70% of the loaded DOXO was released (corresponding to 32.9 μg of DOXO per 1 mg of iron). At 25 °C, the maximum DOXO release was reached after 7 days, and this corresponded to only 25% of the loaded amount (i.e., to 11.8 μg of DOXO per mg of Fe).

To evaluate the drug functionality, a comparative in vitro viability assay, exploiting a PrestoBlue Viability assay, a resazurin-based colorimetric test, was conducted on A431 epidermoid carcinoma cells (Figure 2). For DOXO-loaded-TR-cubes that had been pre-exposed to MH before being added to the cells, the lethal dose of 50% (LD50) was achieved as early as after 24 h of incubation, causing complete cell death after 48 h, whereas the toxic effect of DOXO-loaded-TR-cubes that had not been pre-exposed to MH was seen only after 48 h (Figure 2b for the heat profile of DOXO-loaded-TR-cubes and Figure S8 for the heat profile of cells that had been exposed to AMF without any nanoparticles). The pristine TR-cubes without any loaded drugs showed no effects on the viability even after 48 h of incubation (see also Figure S5d). A confocal analysis on A431 cells after 4 h of exposure to the different TR-cube materials confirmed that only the DOXO-loaded-TR-cubes that had been pre-exposed to MH showed clear signs of drug cytotoxicity, as was clear from a morphological modification of the cells together with a noticeable red signal which confirmed DOXO release and uptake (Figure 2e, third row). In the case of DOXO-loaded-TR-cubes that had not been pre-exposed to MH, the delivery of DOXO was evident from the red signal (which was less intense than that of the DOXO-loaded-TR-cubes that had been pre-exposed to MH), but the amount of chemotherapeutic agent was not high enough to promote cell stress (i.e., the cells did not show any signs of toxicity). It is worth noting that the DOXO alone, after exposure to a warm bath set at 42 or 50 °C, maintained unaltered the same antiproliferating activity as the nonheated DOXO (Figure S9), Overall, these results indicate that MH boosted the release without affecting the chemotherapeutic activity of DOXO, which still maintained its antiproliferating activity against cancer cells, even after exposure to MH.[47]

In Vivo Dual Therapy of Drug-Loaded TR-Cubes Combined with Hyperthermia. In order to verify the in vivo MH efficacy of DOXO-loaded-TR-cubes, an athymic immunodeficient xenograft mouse model induced with A431 cells was used (subcutaneous injection of 1.5×10^6 cells/flank, Figure S10). After tumor growth (80–100 mm^3), the TR-cubes with or without DOXO were intratumorally injected and subjected to three MH cycles (30 min each) over three consecutive days (Figure 3a, 11 KA/m and 110 kHz).

Infrared (IR) images of the mice that had been injected with TR-cubes showed that, during MH1 (day 1 MH), the red spot indicating the high-temperature heat signal was more present at the point of injection than it was after three MH treatments (Figure 3b and Figure S10). During MH3 (day 3 of treatment), the IR signal spread all over the tumor after exposure (Figure 3c). The nanocubes' spreading was also evident in the photograph of the tumor before and after MH (see the enlargements of the black spot at the tumor, Figure 3e).

The temperature difference (ΔT) between the tumor and the skin (which was far from the tumor) was about 15 °C during MH1 and 10 °C during MH2 and MH3 (Figure 3d). To date, this is the highest ΔT reported for such iron oxide MNPs in an in vivo experiment under clinical AMF conditions ($Hf \leq 5 \times 10^9$ A m^{-1} s^{-1}).[48,49]

By monitoring of the tumor growth curves (Figure 3h), it was evident that neither the sole injection of TR-cubes nor DOXO alone could achieve tumor suppression; the DOXO-loaded-TR-cubes in combination with MH (DOXO-loaded-TR-cubes + MH) had the best response, showing complete tumor suppression by day 40. A comparison of tumor suppression between the CTRL and the DOXO-TR-cubes + MH was the most significant with p value 0.0002 (***). There was also a significant difference between the DOXO-TR-cubes and DOXO-TR-cubes + MH with a p value of 0.0035 (**), while the difference between the standard DOXO group and the DOXO-TR-cubes + MH was <0.0001 (****). No reemergence of the tumor mass was observed up to 3 months post-treatment for mice that had been treated with DOXO-loaded-TR-cubes + MH. The survival plot indicated that this same group had the longest survival rate (50% up to 40 days post treatment) among all the groups studied (see Figure 3i), and there were also no signs of fluctuations in body weight (see Figure S10). The standard DOXO treatment was found to be much less effective than the controlled release of DOXO-loaded-TR-cubes + MH (see Figure 3h,i).

To investigate the associated changes in the tumor morphology and the distribution of the TR-cubes and DOXO-loaded-TR-cubes with or without MH, a histopathological analysis was conducted. This analysis indicated that the tumors of the animals that had been treated with TR-cubes alone had thick stromal walls with no sign of collagen disruption (see Fast Red signal in Figure3f and Figure S11 in the Supporting Information). However, the stromal walls were highly diminished, and most of the TR-cubes (Prussian blue staining) were at the periphery of the tumor when it was treated with DOXO-loaded-TR-cubes + MH (see Figure3g). In comparison, when DOXO was injected alone, the stromal thickness was disrupted only in the vicinity of the blood vessels (see Figure S11 in the Supporting Information). Furthermore, a confocal analysis of the tumor slices of this group showed a large spreading of the DOXO signal at the tumor when MH was applied (see Figure3l). For standard chemotherapy (i.v. injection), DOXO signal was observed only at the periphery of the tumor blood vessels (see Figure 3j). It is also worth highlighting the clear difference in cell density (blue, stained using DAPI) between the DOXO-loaded-TR-cubes + MH and the group that had not been exposed to the MH. For those that had been treated with MH, two-thirds of the tumor was black, indicating that the tumor mass lacked viable cells, while the slices of animals that had not been exposed to MH clearly presented a viable tumor (see Figure3k, the blue signal which is spread all over the section, and Figure S12 in the Supporting Information for an overview).

TEM images of the TR-cubes and TR-cubes + HT at the tumor section after 28 days post-injection clearly show the presence of nanocubes inside the endosomes and lysosomes at the tumor cells (Figure S13 in the Supporting Information).

It is also worth highlighting that the dose of nanocubes used here (0.7 mgFe/mouse) is 10–20 times lower than those which have been used with standard spherical iron oxide spherical nanoparticles in previous in vivo efficacy studies.[50,51]
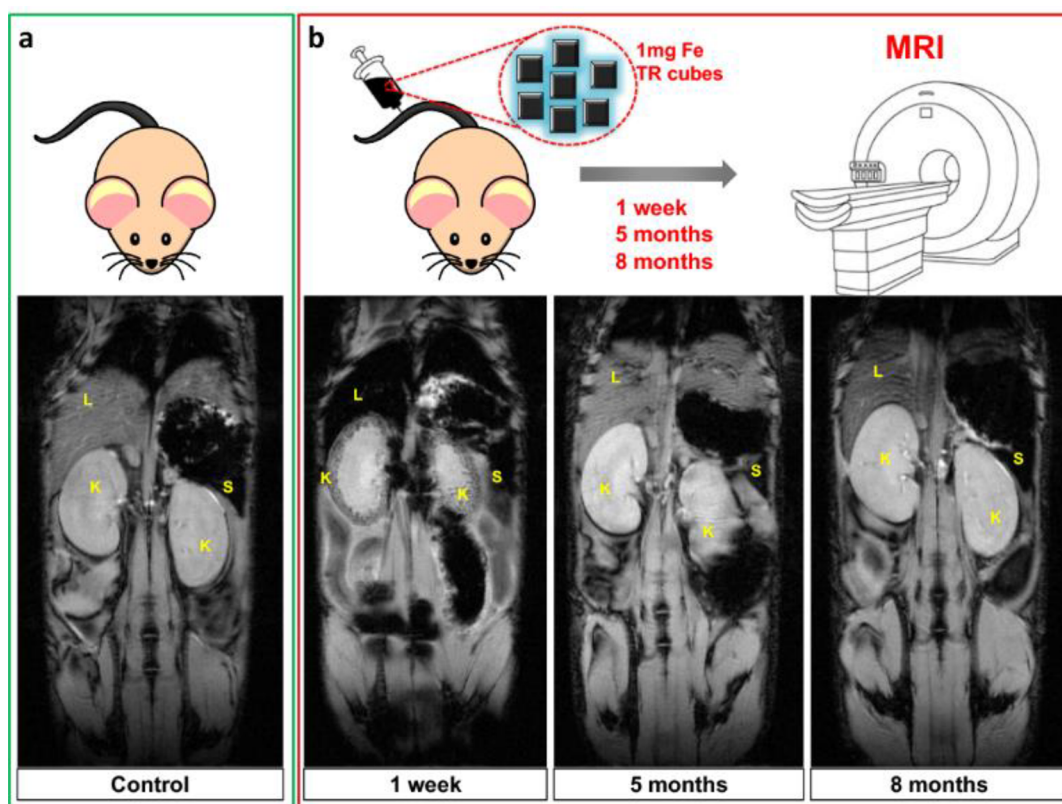
Figure 4. Follow-up of the TR-cube clearance over a period of 8 months after intravenous injection (1 mg iron) in healthy mice. Comparison of gradient echo MRI scans (TE = 10 ms) of a control mouse (a, green panel) and animals injected with 1 mg of Fe containing TR-cubes taken at 1 week, 5 months, and 8 months postinjection (b, red panels). In the last case, a pronounced hypo-intense signal in the liver (L), spleen (S), and kidney (K, note the intense dark spots in kidney cortex) was shown after 1 week, which then disappeared at longer time points, demonstrating the clearance of the magnetic nanoparticles.

Overall, these data suggest that spreading the nanocubes from the point of injection to the periphery under MH contributed to the direct heat damage. It also promoted the spreading of DOXO all over the tumor. Moreover, the nanocube heating likely improved the permeability of the cells/stromal to DOXO, resulting in complete tumor suppression.

In Vivo Biodistribution and Clearance of TR-Cubes. Together with the efficacy, a MRI biodistribution study on healthy mice (with no tumors) provided information on the clearance and biocompatibility of pristine TR-cubes at a relevant dose for hyperthermia. A 1 mg portion of iron per mouse was injected intravenously (i.v.), which corresponds to 1.5 times the dose needed for intratumoral MH. The state of health of the animals was monitored after injection, and MRI was used to obtain images of them at different time points over 8 months. There was a clear liver accumulation (darkened MRI contrast) and initial signs of renal clearance (K, in the kidney cortex) 1 week post-injection, indicating that the material was beginning to eliminate from the body of the animals (see Figure 4).

No MRI signal of nanocubes was observed at the liver or at the kidneys 5−8 months post i.v. injection. In accordance with previously reported data, we might speculate that iron oxide nanocubes can undergo pH degradation in the liver and spleen followed by a sequestration of iron ions by ferritin proteins.[49] The TR polymer shell attached through a catechol moiety to the nanocube surface may detach from the nanocube surface, thus exposing the iron oxide nanocubes to acidic degradation.[49] This may lead to a reduction in the size of the initial nanocubes, enabling excretion by the renal glomerulus. This is, however, only a hypothesis, and further studies should be carried out in the future in order to better clarify the pathway of elimination of the TR-cubes. The TR-cubes are colloidally stable in vivo (no animal died of blood vessel occlusions) and are well tolerated by the animal, as no signs of discomfort were observed throughout the whole 31 weeks of the experiment (see the monitored weight graph, Figure S14 in the Supporting Information). The same MRI trend was observed when the injected TR-cube dose was lowered to 0.5 mg of Fe rather than 1 mg of Fe (see Figure S15 in the Supporting Information).

■ CONCLUSION

To summarize, by exploiting the fast rate of a photoinduced copper-mediated polymerization, we have managed to grow a biocompatible thermoresponsive shell on iron oxide nanocubes in such a way that the outstanding heat performance of these nanocubes is still preserved in both in vitro and in vivo environments (see Figures 1 and 2). The platforms we have developed here enable MH to be combined with chemotherapy using FDA-approved building blocks (DOXO and iron oxide nanoparticles), with the peculiarity that iron oxide nanoparticles are modified in the shape of nanocubes. Notably, the individual components of our platform did not yield the degree of therapeutic efficacy that is required; only by combining them we did attain the highest therapeutic impact (see Figure 3h,i) and the lowest amount of adverse side effects (Figure S10). This, in turn, corresponded to the longest

survival rate for the animals which were treated with DOXO-loeaded-TR-cubes + MH (see Figure 3i). To the best of our knowledge, no other material which is based on a low critical solution temperature thermoresponsive polymer and magnetic nanoparticles has been demonstrated to work in vivo under clinical alternating magnetic field conditions. Moreover, this thermoresponsive polymer nanosystem combines MH and a heat-mediated drug delivery. Many biodistribution studies of iron oxide have been reported for MRI applications at a much lower dosage,[52] but the tolerance colloidal stability and clearance of TR-cubes at the dose needed for MH, which is much higher than that needed for MRI (1 mg/animal in Fe vs 50 μg/animal, respectively) has been shown here (Figure 4). We envision that, upon intratumoral injection, the dual therapeutic action, at a reduced iron dose and with a reasonable biotransformation period, will effectively enable the clearance of our nanoplatforms after MH treatment and drug action. In turn, the nanoplatform degradation will eliminate the interference of the signal of the magnetic nanocubes in MRI and will enable the progression of the tumor to be monitored post-MH-treatment by MRI, an imaging technique that is often chosen by physicians for monitoring the progression of Glioblastoma Multiforme tumors. In addition, our biodistribution study, proving complete tolerance to the TR-cubes and the lack of an MRI signal after a few months, that followed the intravenous injection might pave the way for further studies on these materials under advanced in vivo conditions, such as an intravenous injection of the material used, followed by a magnetic accumulation and MH heat treatment to eradicate cancer. Such a nanoplatform, therefore, has all the features that are required in order to overcome the main limitations of MH in clinic.[28]

■ MATERIALS AND METHODS

Materials. Diethylene glycol methyl ether methacrylate (DEG-MEMA) (Aldrich, 95%) and oligoethylene glycol methyl ether methacrylate (OEGMEMA) (M_w = 500 g mol^{-1}, Aldrich, 99%) were purified from inhibitors by being passed through a basic alumina column. Triethyleneamine (TEA, Aldrich, 99%) was distilled first against *p*-toluenesulfonic acid and then against calcium hydride (CaH$_2$). Dopamine hydrochloride (DOPA·HCl), 2-bromoisobutyryl bromide (2-BiBA), doxorubicin hydrochloride (DOXO), and the specified solvents were purchased from Sigma-Aldrich with the highest available purity and were used as received. Me$_6$TREN was prepared following a published procedure and stored under nitrogen.[53] Cubic iron oxide nanoparticles (cubic-IONPs) were prepared as previously reported.[29,45]

Functionalization of the Nanocube Surface with Initiators by Ligand Exchange. The initiator was immobilized onto the nanoparticle surface by a simple ligand exchange procedure, using an initial ratio of 500 molecules of ligand per nm^2 of nanoparticle surface. In short, for 21.0 nm edge size nanocubes, 120 mg of DOPA-BiBA was dissolved in 12.0 mL of 4% (v/v) methanol in chloroform in a 20 mL vial. To this solution was added 1.5 mL of nanocubes in chloroform (containing 4.0 mg iron), and the suspension was sonicated for 30 s. Subsequently, 55.6 μL of TEA was added to the mixture. The vial was covered with aluminum foil to avoid light exposure and left on the shaker overnight. Next, 15.0 mL of hexane was added to the mixture to precipitate the nanocubes. The suspension was centrifuged for 10 min at 1500 rpm, and the reddish supernatant was discarded. To redisperse the particles, 10 mL of THF was added and the nanocubes were again precipitated in hexane (20 mL). This process was repeated two times to ensure the removal of the free initiator. Then, the DOPA-BiBA-functionalized nanocubes were dispersed in THF (1 mL) to obtain a solution with an iron

concentration of 4.0 g L^{-1}. For the ligand exchange of nanocubes of different sizes, the volume of the reaction (14 mL) was kept constant while the amount of DOPA-BiBA was adjusted to maintain the ratio of 500 molecules per nm^2, and TEA was kept at a 1:1 stoichiometric ratio with respect to DOPA-BiBA.

Synthesis of Nanocubes Functionalized with Thermoresponsive Polymers by Photoinduced Copper Mediated Radical Polymerization (PI-CMRP). A 1.5 mL portion of DOPA-BiBA functionalized nanocubes in THF ([Fe] = 4.0 g L^{-1}) was diluted with 4.5 mL of DMSO to form a clear solution. Afterward, a mixture containing 7.5 mL of DMSO, 720 μL of OEGMEMA, and 1345 μL of DEGMEMA was slowly added (drop by drop) to this solution. Four samples of the above mixture were prepared separately and then combined together in one cylindrical open-capped flask (diameter 100.0 cm, height 35.0 cm). This solution was sonicated for 30 s at room temperature and purged with nitrogen for 15 min (it is enough to purge with nitrogen rather than work under freezing/thawing cycles, that is to apply multiple vacuum/nitrogen cycles). Next, 6.0 mL of a catalyst stock solution containing 6.0 mL of DMSO, 0.80 mg of CuBr$_2$ and 1.92 μL of Me$_6$TREN was successively injected into the vial. To initiate the polymerization, the vial was kept in a cold room set at 5 °C and exposed to a UV source. A UV nail gel curing lamp (λ_{max} ∼360 nm) equipped with four 9 W bulbs was used as the UV light source. During the polymerization, the reactor was shaken with an orbital shaker (speed 100 rpm). After 2.5 h of irradiation, the polymerization was quenched by adding 80 mL of THF and by being exposed to air. The nanoparticles were precipitated in diethyl ether, resulting in a black gel-like precipitate. The dissolution in THF and precipitation in diethyl ether were repeated two times, and the final precipitate was dried by nitrogen flow and redispersed in 60 mL of deionized water. The sample was concentrated to a final volume of 20 mL by filter centrifugation. To remove the excess polymeric ligands, this solution was subjected to ultracentrifugation using the following conditions: sucrose gradient in 12 mL tubes, 2 mL 66% (w/w)−3 mL 40% (w/w)−3 mL 20% (w/w), speed 25000 rpm for 45 min. The speed used for the ultracentrifugation varied slightly depending on the core size of the nanocubes. For TR-cubes with larger core sizes, a slower speed was required. The TR-cube fraction was collected at the middle of the centrifugation tubes, while the layer on top containing unbounded polymers was collected and lyophilized for size exclusion chromatography (SEC) measurements and ^{1}H NMR spectroscopy. The sucrose was removed by filter centrifugation, and the stable TR-cubes were transferred into phosphate-buffered saline or pure saline for further characterization.

DOXO Loading in Saline. The encapsulation of DOXO into the thermoresponsive polymer shell of TR-cubes was accomplished by simple incubation. In short, 400 μL of TR-cubes in saline (5.0 g L^{-1}, 2.0 mg iron) was added to 19.0 mL of a saline solution (0.9% NaCl) containing 1 mg of DOXO, and the mixture was sonicated for 10 s. By addition of more of the saline solution, the volume was increased to 20 mL, and this solution was then transferred into a 40 mL vial after further sonication for 20 s. The vial was covered with aluminum foil and gently shaken for 16 h. After incubation, the magnetic TR-cubes were isolated from the solution by magnetic decantation. Figure S5b shows the spectra of the supernatants upon the washing steps. The TR-cubes loaded with DOXO were washed three times by magnetic decantation, using saline as fresh media. After the last washing step, an appropriate amount of saline was added to yield a dark reddish solution with an iron concentration of 2.5 g L^{-1}.

Protein Absorption Test. To investigate their interaction with biomolecules, the TR-cubes were incubated in 10% fetal bovine serum (FBS) or 10% human serum in PBS at a concentration of 0.2 mg of Fe mL^{-1}. The samples were incubated for 90 min at 37 °C and then collected by centrifugation at 14000 rpm for 30 min. The pellet was resuspended and washed in PBS three times through gentle pipetting to remove any unbound proteins.[54] Then, the proteins were eluted by resuspending the samples in a 5× loading sample buffer and heated to 100 °C for 5 min. The buffer was prepared following the recipe reported elsewhere.[55] Gel electrophoresis was performed on a 12% polyacrylamide gel at 120 V for 1 h. Control samples of bare FBS and

human serum were prepared with the same protocol as that used for the TR-cubes and were loaded into the gel. Novex Sharp Prestained Protein Standard from Invitrogen was used as a molecular ladder (4 μL). The same volume of all samples (16 μL) was added to allow a direct comparison of the results. The gel was stained with Coomassie Blue dye for 30 min and then distained overnight in water for analysis using BIO-RAD ChemiDOC MP equipment.

Cell Culture. A431 epidermoid carcinoma cells (ATCC CRL-1555) were cultured in Dulbecco's Modified Eagle's Medium (DMEM, high glucose) supplemented with 10% fetal bovine serum (heat inactivated FBS), 2% penicillin–streptamycin (10000 U/mL), and 1% L-glutamine (200 mM) at 37 °C, 5% CO_2, and 95% relative humidity. All of the cell culture reagents were purchased from Gibco.

In Vitro Cytotoxicity Assay. A431 cells were plated in 24-multiwell plates and allowed to reach a confluence state. A 50 μL portion of TR-cubes (2.5 g·L^{-1} Fe) and 50 μL of the same sample loaded with DOXO (DOXO-loaded TR-cubes, 42 μg of DOXO/1 mg of Fe) were exposed to an alternating magnetic field of 11 kA/m and to a frequency of 105 kHz for 90 min (3 exposures of 30 min each, mimicking the conditions to be used in further in vivo experiments) using an MH setup (DM1 applicator, DM100 series for calorimetry, nb nanoScale Biomagnetics). Under AMF, the TR-cubes and DOXO-loaded-TR-cubes reached 43 °C, the MH temperature, which was also above the lower critical solution temperature (LCST) of the thermoresponsive polymer that was used. Under another set of conditions, the TR-cubes and DOXO-loaded-TR-cubes (both without prior MH treatments) were also taken as comparison groups (using the same concentrations as for the MH-treated samples). Then the TR-cubes alone, DOXO-loaded-TR-cubes alone, MH-treated TR-cubes, and MH-treated DOXO-loaded-TR-cubes were further diluted 10 times with media and incubated with the cells for 24 and 48 h. The control group (Ctrl) consisted of cells grown under normal culture conditions. After the incubation periods, a cytotoxicity assay was conducted using PrestoBlue Cell Viability Reagent (Invitrogen), using the same conditions described in the previous section. The experiment was done in triplicate ($n = 3$), and the mean value was plotted with an error bar to represent the SD. The same experiment was also repeated with a lower concentration of DOXO-loaded-TR-cubes (1.5 g L^{-1}), again in triplicate. The statistics calculations within multiple groups were done using two-way ANOVA and Tukey's multiple comparison test with 95% confidence interval in Graphpad.

Confocal Analysis. For confocal analysis, the A431 cells were cultured over a glass coverslip placed in a 24-well plate and treated with non-MH- or MH-treated DOXO-loaded-TR-cubes for 4 h. In the case of the MH-treated DOXO-loaded-TR-cubes, 50 μL of 2.5 g L^{-1} of the sample was first pre-exposed to AMF and further diluted 10 times (0.25 g L^{-1}) before incubating with the cells. For DOXO-loaded-TR-cubes (no MH), 500 μL of 0.25 g L^{-1} of the sample was directly incubated with cells. After 4 h, the cells were washed three times with PBS to remove the noninternalized DOXO and magnetic materials. The cells were then tagged with Hoechst 33342 nuclear staining solution (ThermoFisher Scientific) and fixed with 4% paraformaldehyde. The coverslips were then carefully lifted off from the well plates and fixed over a glass slide. The prepared slides were viewed using a confocal microscope ($A1^+$ confocal microscope system, Nikon) at an excitation/emission wavelength of 350/461 nm for Hoechst (blue) and 470/585 nm for doxorubicin hydrochloride (red).

Mouse Strain and Tumor Model. Pathogen-free female, 8 weeks old immunodeficient athymic NMRI-nude (Crl:NMRI-Foxn1nu, Outbred) mice were used throughout the study. They were housed in IVC cages in a temperature-controlled room with a 12 h/12 h dark/light cycle, with ad libitum access to water and food. Animal health and comfort were veterinary-controlled regularly. All animal experiments were performed in full compliance with Italian law d.lgs 116/92 (EU Directive 2010/63/EU for animal experiments) and the Istituto Italiano di Tecnologia (IIT) Ethical Committee.

For the tumor model, A431 epidermoid carcinoma cells cultured to 70% confluency were used using the aforementioned method. The mice were injected subcutaneously with 1.5 × 10^6 A431 cells in 100 μL of saline in one of their flanks. This step was done under anesthesia, which was induced via a VetEquip Inhalation anesthesia system using isoflurane (IsoVet: 0.8–1.5 L/min concentration 2–3%). This ensured an easy and uninterrupted injection of the cancer cells subcutaneously without inflicting any pain or distress to the animals. The animals were then placed in their respective cages (five animals per cage) and weighed and monitored every 3 days for tumor growth.

Grouping of Animals. (1) Control animals just carrying a tumor (no TR-cubes injection): six animals (CTRL). (2) Animals injected with 50 μL of $14g_{Fe}$/L TR-cubes alone (0.7 mg Fe per mouse): six animals (TR-cubes). (3) Animals injected with 50 μL of 14g/L DOXO-loaded TR-cubes (23.3 μg DOXO and 0.7 mg Fe per mouse): six animals (DOXO-loaded-TR-cubes). (4) Animals injected with 50 μL of 14 g/L TR-cubes alone and subjected to three cycles of MH: six animals (TR-cubes + MH). (5) Animals injected with 50 μL of 14 g/L DOXO-loaded-TR-cubes and subjected to three cycles of MH: six animals (DfourOXO-loaded TR-cubes + MH). (6) Animals representing standard chemotherapy treatments injected with DOXO in 50 μLof saline (20 mg/kg body weight): four animals (standard DOXO). Animals injected with a DOXO amount in correspondence to the loaded DOXO in the TR-cubes (23.3 μg in 50 μL of saline): four animals (DOXO*).

TR-cube Injection and Hyperthermia Treatments. When the tumor volume reached approximately 80–100 mm^3, the animals were injected intratumorally with the nanocubes (TR-cubes or DOXO-loaded-TR-cubes) using a hypodermic syringe fitted to a needle (BD insulin syringe with BD Ultra-Fine 6 mm needle; 30G, 0.5 mL). Prior to the particle injection, the animals were anesthetized using an intraperitoneal injection of a ketamine–xylazine solution mixture (70–100 and 5–10 mg/kg, respectively). The amount of ketamine–xylazine administration was adjusted on the basis of the body weight of the individual animals (80 μL per 20 g of body weight). This general anesthesia dosage ensured that the animals had a complete loss of consciousness for 30–40 min, which facilitated a precise intratumoral injection of the MNPs and the following 30 min MH cycle. The first cycle of MH (MH1) was started immediately after the particle injection, whereas MH2 and MH3 were on the following consecutive days. The frequency, field, and exposure conditions used were 110 kHz, 11 kA/m, and 30 min, respectively (NAN201003 MagneTherm nanoTherics Ltd.). The field and frequency range used was well within the ethically accepted AMF limits. During the treatment, the temperature of the animals was monitored using an IR camera (Fluka Inc.), which was then used to determine the ΔT value ($\Delta T = T_{tumor} - T_{skin}$). For the standard DOXO and DOXO* groups, respective DOXO amounts in 100 μL of saline were injected intravenously while the animals were painlessly constrained.

Tumor Growth Curve. The tumor volumes (V) were measured using a Vernier caliper and calculated using the formula $V = ((\text{long diameter}) \times (\text{short diameter})^2)/2.$[56] Then the mean of the tumor volume with the SD of all animals per group was plotted against the number of days since the particle injection and MH1.

Survival curve. Whenever an animal was sacrificed due to the humane end point (10% increase in body weight and a tumor length greater than 2 cm) or other incidences, the number of dead animals was recorded using the Kaplan–Meier survival data plot in GraphPad (noted 1 for death post humane end point and 0 for the death due to other incidence).

TR-cube Injection for Biodistribution Studies. Pristine TR-cubes in 100 μL of saline at concentrations of 0.5 mg of Fe ($n = 8$) and 1 mg of Fe ($n = 8$) were injected into the tail vein intravenously. For control purposes, other animals were injected with 100 μL of just saline solution ($n = 4$). The animals were then monitored by weighing them periodically and checking for any physical or mental distress. MRI images were obtained at 1 weeks, 5 months, and 9 months post MNP injection.

MRI Imaging. The MRI was performed on a 4.7 T preclinical MRI scanner (BioSpec 47/40 USR) interfaced with ParaVision software (both provided from Bruker Biospin GmbH, Rheinstetten, Germany)

at the Plateforme Imageries du Vivant of Paris Descartes (PARCC-HEGP, INSERM UMR 970, University Paris Descartes, Sorbonne Paris Cité, Faculté de médecine, Paris, France). The shole body imaging protocol was performed with a volume transmission/reception rf coil for mice with an inner diameter of 3.5 cm (Bruker). The nanoparticle biodistribution was monitored using a gradient echo sequence (repetition time 300 ms), two different echo times (TE = 5 or 10 ms, flip angle 30°, field of view 5 × 4 cm, eight averages, and a pixel resolution of 156 × 156 μm) with coronal slices (thickness 1 mm) being positioned over the liver, spleen, kidneys, and bladder. A tube of water was placed with the mouse and was used as a signal reference. The whole body imaging protocol was performed on control noninjected mice (n = 4), 1 week (n = 2), 5 months (n = 3), and 8 months (n = 3) postinjection of the nanoparticles (TR-cube doses equal to 1 or 0.5 mg of iron). The mean MRI signal (S) was measured in the region of interest (ROI), encompassing the different organs of interest and normalizing the signal of the water reference tube. In the liver, ROIs were drawn around apparent vascular structures and these regions were subtracted from the map to retain liver parenchyma only. Regions of interest encompassing the whole spleen or the two kidneys or the kidney cortex were manually selected for signal measurements.

Statistics. For in vitro studies, n = 3 and the statistics calculations within multiple groups were done using two-way ANOVA and Tukey's multiple comparison test with 95% confidence interval in Graphpad. Significant differences were reported as ***p = 0.0001−0.001 and ****p < 0.0001. Due to the exploratory nature of the in vivo testing after successful results obtained in in vitro studies, we decided after consultation with experienced personnel the n value to be 6 for this study. The sample size used was not chosen to detect a prespecified effect size. The animals that did not successfully grow tumors were eliminated from the study prior to testing the nanoparticle platform. Randomization was used to allocate animals in different groups for the nude mice xenograft of A431 cells. The survival analysis of the animals was done using a Kaplan−Meier survival plot in GraphPad.

For the tumor growth curve, the mean and SD of the normalized tumor volume at the end point of each group was analyzed to the CTRL untreated tumor end point using an unpaired nonparametric t test.

ASSOCIATED CONTENT

Ⓢ Supporting Information

The Supporting Information is available free of charge on the ACS Publications Web site at DOI: The Supporting Information is available free of charge on the ACS Publications website at DOI: 10.1021/acsami.8b16226.

Experimental details and additional data as described in the text (PDF)

AUTHOR INFORMATION

Corresponding Author

*E-mail: for T.P.: Teresa.pellegrino@iit.it.

ORCID Ⓞ

Binh T. Mai: 0000-0002-3418-0658
Preethi B. Balakrishnan: 0000-0001-5576-7530
Florence Gazeau: 0000-0002-6482-3597
Teresa Pellegrino: 0000-0001-5518-1134

Present Address

#The Gurdon Institute and Dept. of Biochemistry, University of Cambridge, Tennis Court Road, Cambridge CB2 1QN, U.K.

Author Contributions

⊥B.T.M. and P.B.B. contributed equally to this work.

Author Contributions

T.P., B.T.M., and P.B.B. conceived and designed the experiments, B.T.M., T.P., M.J.B., H.K., and R.C. developed the material, P.B.B., D.N., S.F., and A.C. performed in vitro experiments, P.B.B., F.P., F.M., F.G., and G.A. performed the in vivo experiments, and T.P., B.T.M. and P.B.B. cowrote the paper with contributions obtained from all authors.

Notes

The authors declare the following competing financial interest(s): Teresa Pellegrino, Thanh Binh Mai, Preethi Bala Balakrishnan, Markus Barthel, Hamilton Kakwere, and Roberto Cingolani are coinventors of an Italian priority application (pending) IT 102017000009221; Pellegrino et al.; "Procedimento per la sintesi di nanoparticelle magnetiche stimolo-responsive"; filing date January 27, 2017; and the International extension PCT/IB2017/050477; Pellegrino et al.; "Process for the synthesis of magnetic stimuli-responsive nanoparticles"; filing date January 26, 2018.

ACKNOWLEDGMENTS

REFERENCES

(1) Andocs, G.; Szasz, O.; Szasz, A. Oncothermia treatment of cancer: from the laboratory to clinic. *Electromagn. Biol. Med.* **2009**, *28*, 148−165.

(2) Mahmoudi, K.; Bouras, A.; Bozec, D.; Ivkov, R.; Hadjipanayis, C. Magnetic hyperthermia therapy for the treatment of glioblastoma: a review of the therapy's history, efficacy, and application in humans. *Int. J. Hyperthermia* **2018**, *34*, 1316−1328.

(3) Dewhirst, M. W.; Lee, C.-T.; Ashcraft, K. A. The future of biology in driving the field of hyperthermia. *Int. J. Hyperthermia* **2016**, *32*, 4−13.

(4) Keizer, H.; Pinedo, H.; Schuurhuis, G.; Joenje, H. Doxorubicin (adriamycin): a critical review of free radical-dependent mechanisms of cytotoxicity. *Pharmacol. Ther.* **1990**, *47*, 219−231.

(5) Salmon, S. E.; Grogan, T. M.; Miller, T.; Scheper, R.; Dalton, W. S. Prediction of doxorubicin resistance in vitro in myeloma, lymphoma, and breast cancer by P-glycoprotein staining. *JNCI: J. Natl. Cancer Inst.* **1989**, *81*, 696−701.

(6) Singal, P. K.; Iliskovic, N.; Li, T.; Kumar, D. Adriamycin cardiomyopathy: pathophysiology and prevention. *FASEB J.* **1997**, *11*, 931−936.

(7) Jiang, W.; Lionberger, R.; Yu, L. X. In vitro and in vivo characterizations of PEGylated liposomal doxorubicin. *Bioanalysis* **2011**, *3*, 333−344.

(8) Meirow, D.; Nugent, D. The effects of radiotherapy and chemotherapy on female reproduction. *Hum. Reprod. Update* **2001**, *7*, 535−543.

(9) Wust, P.; Hildebrandt, B.; Sreenivasa, G.; Rau, B.; Gellermann, J.; Riess, H.; Felix, R.; Schlag, P. Hyperthermia in combined treatment of cancer. *Lancet Oncol.* **2002**, *3*, 487−497.

(10) Van der Zee, J. Heating the patient: a promising approach? *Ann. Oncol.* **2002**, *13*, 1173−1184.

(11) Issels, R. D.; Lindner, L. H.; Verweij, J.; Wust, P.; Reichardt, P.; Schem, B.-C.; Abdel-Rahman, S.; Daugaard, S.; Salat, C.; Wendtner, C.-M. Neo-adjuvant chemotherapy alone or with regional hyperthermia for localised high-risk soft-tissue sarcoma: a randomised phase 3 multicentre study. *Lancet Oncol.* **2010**, *11*, 561−570.

(12) Hilger, I. In vivo applications of magnetic nanoparticle hyperthermia. *Int. J. Hyperthermia* **2013**, *29*, 828−834.

(13) Mai, B. T.; Fernandes, S.; Balakrishnan, P. B.; Pellegrino, T. Nanosystems Based on Magnetic Nanoparticles and Thermo- or pH-Responsive Polymers: An Update and Future Perspectives. *Acc. Chem. Res.* **2018**, *51*, 999−1013.

(14) Stuart, M. A. C.; Huck, W. T.; Genzer, J.; Müller, M.; Ober, C.; Stamm, M.; Sukhorukov, G. B.; Szleifer, I.; Tsukruk, V. V.; Urban, M. Emerging applications of stimuli-responsive polymer materials. *Nat. Mater.* **2010**, *9*, 101.

(15) Mura, S.; Nicolas, J.; Couvreur, P. Stimuli-responsive nanocarriers for drug delivery. *Nat. Mater.* **2013**, *12*, 991.

(16) Xu, R.; Zhang, G.; Mai, J.; Deng, X.; Segura-Ibarra, V.; Wu, S.; Shen, J.; Liu, H.; Hu, Z.; Chen, L. An injectable nanoparticle generator enhances delivery of cancer therapeutics. *Nat. Biotechnol.* **2016**, *34*, 414.

(17) Lee, N.; Yoo, D.; Ling, D.; Cho, M. H.; Hyeon, T.; Cheon, J. Iron oxide based nanoparticles for multimodal imaging and magnetoresponsive therapy. *Chem. Rev.* **2015**, *115*, 10637−10689.

(18) Johannsen, M.; Thiesen, B.; Wust, P.; Jordan, A. Magnetic nanoparticle hyperthermia for prostate cancer. *Int. J. Hyperthermia* **2010**, *26*, 790−795.

(19) Colombo, M.; Carregal-Romero, S.; Casula, M. F.; Gutiérrez, L.; Morales, M. P.; Böhm, I. B.; Heverhagen, J. T.; Prosperi, D.; Parak, W. J. Biological applications of magnetic nanoparticles. *Chem. Soc. Rev.* **2012**, *41*, 4306−4334.

(20) Yassine, O.; Zaher, A.; Li, E. Q.; Alfadhel, A.; Perez, J. E.; Kavaldzhiev, M.; Contreras, M. F.; Thoroddsen, S. T.; Khashab, N. M.; Kosel, J. Highly efficient thermoresponsive nanocomposite for controlled release applications. *Sci. Rep.* **2016**, *6*, 28539.

(21) Kakwere, H.; Leal, M. P.; Materia, M. E.; Curcio, A.; Guardia, P.; Niculaes, D.; Marotta, R.; Falqui, A.; Pellegrino, T. Functionalization of strongly interacting magnetic nanocubes with (thermo) responsive coating and their application in hyperthermia and heat-triggered drug delivery. *ACS Appl. Mater. Interfaces* **2015**, *7*, 10132−10145.

(22) Thomas, C. R.; Ferris, D. P.; Lee, J.-H.; Choi, E.; Cho, M. H.; Kim, E. S.; Stoddart, J. F.; Shin, J.-S.; Cheon, J.; Zink, J. I. Noninvasive remote-controlled release of drug molecules in vitro using magnetic actuation of mechanized nanoparticles. *J. Am. Chem. Soc.* **2010**, *132*, 10623−10625.

(23) Sun, C.; Lee, J. S.; Zhang, M. Magnetic nanoparticles in MR imaging and drug delivery. *Adv. Drug Delivery Rev.* **2008**, *60*, 1252−1265.

(24) Hu, S.-H.; Liu, T.-Y.; Huang, H.-Y.; Liu, D.-M.; Chen, S.-Y. Magnetic-sensitive silica nanospheres for controlled drug release. *Langmuir* **2008**, *24*, 239−244.

(25) Hergt, R.; Dutz, S.; Müller, R.; Zeisberger, M. Magnetic particle hyperthermia: nanoparticle magnetism and materials development for cancer therapy. *J. Phys.: Condens. Matter* **2006**, *18*, S2919.

(26) Kobayashi, T. Cancer hyperthermia using magnetic nanoparticles. *Biotechnol. J.* **2011**, *6*, 1342−1347.

(27) Häfeli, U. O.; Chastellain, M. Magnetic nanoparticles as drug carriers. In *Nanoparticulates as Drug Carriers*; World Scientific: 2006; pp 397−418.

(28) Thiesen, B.; Jordan, A. Clinical applications of magnetic nanoparticles for hyperthermia. *Int. J. Hyperthermia* **2008**, *24*, 467−474.

(29) Guardia, P.; Di Corato, R.; Lartigue, L.; Wilhelm, C.; Espinosa, A.; Garcia-Hernandez, M.; Gazeau, F.; Manna, L.; Pellegrino, T. Water-soluble iron oxide nanocubes with high values of specific absorption rate for cancer cell hyperthermia treatment. *ACS Nano* **2012**, *6*, 3080−3091.

(30) Alphandery, E.; Faure, S.; Seksek, O.; Guyot, F. O.; Chebbi, I. N. Chains of magnetosomes extracted from AMB-1 magnetotactic bacteria for application in alternative magnetic field cancer therapy. *ACS Nano* **2011**, *5*, 6279−6296.

(31) Materia, M. E.; Guardia, P.; Sathya, A.; Pernia Leal, M.; Marotta, R.; Di Corato, R.; Pellegrino, T. Mesoscale Assemblies of Iron Oxide Nanocubes as Heat Mediators and Image Contrast Agents. *Langmuir* **2015**, *31*, 808−816.

(32) Cabrera, D.; Lak, A.; Yoshida, T.; Materia, M. E.; Ortega, D.; Ludwig, F.; Guardia, P.; Sathya, A.; Pellegrino, T.; Teran, F. J. Unraveling viscosity effects on the hysteresis losses of magnetic nanocubes. *Nanoscale* **2017**, *9*, 5094−5101.

(33) Zetterlund, P. B.; Thickett, S. C.; Perrier, S. B.; Bourgeat-Lami, E.; Lansalot, M. Controlled/living radical polymerization in dispersed systems: an update. *Chem. Rev.* **2015**, *115*, 9745−9800.

(34) Discekici, E. H.; Anastasaki, A.; Kaminker, R.; Willenbacher, J.; Truong, N. P.; Fleischmann, C.; Oschmann, B.; Lunn, D. J.; Read de Alaniz, J.; Davis, T. P. Light-Mediated Atom Transfer Radical Polymerization of Semi-Fluorinated (Meth) acrylates: Facile Access to Functional Materials. *J. Am. Chem. Soc.* **2017**, *139*, 5939−5945.

(35) Chen, M.; Zhong, M.; Johnson, J. A. Light-controlled radical polymerization: Mechanisms, methods, and applications. *Chem. Rev.* **2016**, *116*, 10167−10211.

(36) Anastasaki, A.; Nikolaou, V.; Zhang, Q.; Burns, J.; Samanta, S. R.; Waldron, C.; Haddleton, A. J.; McHale, R.; Fox, D.; Percec, V. Copper (II)/tertiary amine synergy in photoinduced living radical polymerization: Accelerated synthesis of ω-functional and α, ω-heterofunctional poly (acrylates). *J. Am. Chem. Soc.* **2014**, *136*, 1141−1149.

(37) Laun, J.; Vorobii, M.; de los Santos Pereira, A.; Pop Georgievski, O.; Trouillet, V.; Welle, A.; Barner Kowollik, C.; Rodriguez Emmenegger, C.; Junkers, T. Surface Grafting via Photo Induced Copper Mediated Radical Polymerization at Extremely Low Catalyst Concentrations. *Macromol. Rapid Commun.* **2015**, *36*, 1681−1686.

(38) Chuang, Y.-M.; Ethirajan, A.; Junkers, T. Photoinduced sequence-controlled copper-mediated polymerization: synthesis of decablock copolymers. *ACS Macro Lett.* **2014**, *3*, 732−737.

(39) Zoppe, J. O.; Ataman, N. C.; Mocny, P.; Wang, J.; Moraes, J.; Klok, H.-A. Surface-initiated controlled radical polymerization: state-of-the-art, opportunities, and challenges in surface and interface engineering with polymer brushes. *Chem. Rev.* **2017**, *117*, 1105−1318.

(40) Zhang, J.; Srivastava, R.; Misra, R. Core− shell magnetite nanoparticles surface encapsulated with smart stimuli-responsive polymer: Synthesis, characterization, and LCST of viable drug-targeting delivery system. *Langmuir* **2007**, *23*, 6342−6351.

(41) Johannsen, M.; Gneveckow, U.; Eckelt, L.; Feussner, A.; Waldöfner, N.; Scholz, R.; Deger, S.; Wust, P.; Loening, S.; Jordan, A. Clinical hyperthermia of prostate cancer using magnetic nano-particles: presentation of a new interstitial technique. *Int. J. Hyperthermia* **2005**, *21*, 637−647.

(42) Hervault, A.; Dunn, A. E.; Lim, M.; Boyer, C.; Mott, D.; Maenosono, S.; Thanh, N. T. Doxorubicin loaded dual pH-and thermo-responsive magnetic nanocarrier for combined magnetic hyperthermia and targeted controlled drug delivery applications. *Nanoscale* **2016**, *8*, 12152−12161.

(43) N'Guyen, T. T.; Duong, H. T.; Basuki, J.; Montembault, V.; Pascual, S.; Guibert, C.; Fresnais, J.; Boyer, C.; Whittaker, M. R.; Davis, T. P. Functional Iron Oxide Magnetic Nanoparticles with Hyperthermia Induced Drug Release Ability by Using a Combination of Orthogonal Click Reactions. *Angew. Chem., Int. Ed.* **2013**, *52*, 14152−14156.

(44) Guardia, P.; Riedinger, A.; Kakwere, H.; Gazeau, F.; Pellegrino, T. *Magnetic Nanoparticles for Magnetic Hyperthermia and Controlled Drug Delivery*; Wiley: 2014; pp 139−172.

(45) Guardia, P.; Riedinger, A.; Nitti, S.; Pugliese, G.; Marras, S.; Genovese, A.; Materia, M. E.; Lefevre, C.; Manna, L.; Pellegrino, T. One pot synthesis of monodisperse water soluble iron oxide nanocrystals with high values of the specific absorption rate. *J. Mater. Chem. B* **2014**, *2*, 4426−4434.

(46) Gombotz, W. R.; Guanghui, W.; Horbett, T. A.; Hoffman, A. S. Protein adsorption to poly (ethylene oxide) surfaces. *J. Biomed. Mater. Res.* **1991**, *25*, 1547−1562.

(47) Cazares-Cortes, E.; Espinosa, A.; Guigner, J.-M.; Michel, A.; Griffete, N.; Wilhelm, C.; Ménager, C. Doxorubicin intracellular remote release from biocompatible oligo (ethylene glycol) methyl

ether methacrylate-based magnetic Nanogels triggered by magnetic hyperthermia. *ACS Appl. Mater. Interfaces* **2017**, *9*, 25775−25788.

(48) Cho, M.; Cervadoro, A.; Ramirez, M. R.; Stigliano, C.; Brazdeikis, A.; Colvin, V. L.; Civera, P.; Key, J.; Decuzzi, P. Assembly of Iron Oxide Nanocubes for Enhanced Cancer Hyperthermia and Magnetic Resonance Imaging. *Nanomaterials* **2017**, *7*, 72.

(49) Kolosnjaj-Tabi, J.; Di Corato, R.; Lartigue, L.; Marangon, I.; Guardia, P.; Silva, A. K.; Luciani, N.; Clément, O.; Flaud, P.; Singh, J. V. Heat-generating iron oxide nanocubes: subtle "destructurators" of the tumoral microenvironment. *ACS Nano* **2014**, *8*, 4268−4283.

(50) Attaluri, A.; Ma, R.; Qiu, Y.; Li, W.; Zhu, L. Nanoparticle distribution and temperature elevations in prostatic tumours in mice during magnetic nanoparticle hyperthermia. *Int. J. Hyperthermia* **2011**, *27*, 491−502.

(51) Dutz, S.; Kettering, M.; Hilger, I.; Müller, R.; Zeisberger, M. Magnetic multicore nanoparticles for hyperthermia—influence of particle immobilization in tumour tissue on magnetic properties. *Nanotechnology* **2011**, *22*, 265102.

(52) Sharma, A.; Cornejo, C.; Mihalic, J.; Geyh, A.; Bordelon, D. E.; Korangath, P.; Westphal, F.; Gruettner, C.; Ivkov, R. Physical characterization and in vivo organ distribution of coated iron oxide nanoparticles. *Sci. Rep.* **2018**, *8*, 4916.

(53) Basuki, J. S.; Esser, L.; Zetterlund, P. B.; Whittaker, M. R.; Boyer, C.; Davis, T. P. Grafting of P (OEGA) onto magnetic nanoparticles using Cu (0) mediated polymerization: comparing grafting "from" and "to" approaches in the search for the optimal material design of nanoparticle MRI contrast agents. *Macromolecules* **2013**, *46*, 6038−6047.

(54) Monopoli, M. P.; Pitek, A. S.; Lynch, I.; Dawson, K. A. Formation and characterization of the nanoparticle−protein corona. In *Nanomaterial Interfaces in Biology*; Springer: 2013; pp 137−155.

(55) Laemmli, U. K. Cleavage of structural proteins during the assembly of the head of bacteriophage T4. *Nature* **1970**, *227*, 680.

(56) Faustino-Rocha, A.; Oliveira, P. A.; Pinho-Oliveira, J.; Teixeira-Guedes, C.; Soares-Maia, R.; Da Costa, R. G.; Colaco, B.; Pires, M. J.; Colaço, J.; Ferreira, R. Estimation of rat mammary tumor volume using caliper and ultrasonography measurements. *Lab. Anim.* **2013**, *42*, 217.